Research Article

Establishment of Thermal Ductile Fracture Criterion for As-Cast 42CrMo Steel and Its Application in Hot Ring Rolling Process

Yuanyuan Chen [ID],[1,2] **Huiping Qi** [ID],[1] **Yongtang Li,**[1] **and Lin Hua**[3]

[1]*School of Materials Science and Engineering, Taiyuan University of Science and Technology, Taiyuan, Shanxi 030024, China*
[2]*Department of Mechanics, Jinzhong University, Jinzhong, Shanxi 030600, China*
[3]*School of Automotive Engineering, Wuhan University of Technology, Wuhan, Hubei 430070, China*

Correspondence should be addressed to Huiping Qi; qhp9974@tyust.edu.cn

The casting-rolling compound forming process of ring parts is an advanced plastic forming technology that has been developed due to the merits of high efficiency and energy and material saving. However, cracks often occur during the hot ring rolling process, especially at the edges of the ring parts, which severely affects the forming quality. To predict and try to avoid the occurrence of cracks in the casting-rolling compound forming process of ring parts, the high-temperature fracture behaviors of as-cast 42CrMo steel were investigated by thermodynamic experiment method. The high-temperature tensile tests were carried out using the Gleeble-3500D thermomechanical simulator at various temperatures and strain rates. Stress-strain curves and fracture morphology were examined, through which the sensitivity of stress to temperature and strain rate and the effect of dynamic recrystallization and cavity evolution on fracture were found. The law of critical fracture strains was analyzed, and the model of critical fracture strain as a function of temperature and strain rate was established. Based on Oyane criterion, the thermal ductile fracture criterion was established in conjunction with the model of critical fracture strain. By embedding this thermal damage model into the finite element (FE) model for hot ring rolling of an as-cast 42CrMo ring, the damage prediction for this process was realized, and the thermal ductile fracture criterion was proved to be reliable. From the FE results for hot ring rolling, mechanism of damage and fracture in the hot ring rolling process was analyzed. The damage threshold C_f is small, and the damage ratio D is large at the top and bottom edges of the inner surface area of the ring, which have the greatest propensity to cracking in the course of hot ring rolling. This is of great significance in terms of improving the forming quality of ring parts in the casting-rolling compound forming process.

1. Introduction

The casting-rolling compound forming process of ring parts is a new technology with many merits such as high efficiency, energy and material saving, and reduction of carbon dioxide emission. In such process, a ring casting blank is rolled directly on a ring rolling machine without being forged. Unfortunately, cracks often occur during the ring rolling, especially at the edges of the ring parts, which seriously affects their quality. In order to improve the forming quality and forming limit of the ring parts, it is vital to predict when and where the cracks initiate in the casting-rolling compound forming process of ring parts.

In the previous research, remarkable results on crack prediction were achieved. Many ductile fracture criteria were proposed to describe the critical conditions of ductile fracture quantitatively with considering the effects of deformation temperature and strain rate on fracture. In particular, the ductile fracture criteria were established for Mn18Cr18N steel [1], 3Cr20Ni10W2 alloy [2], Ti40 alloy [3], 30Cr2Ni4-MoV ultra-super-critical rotor steel [4], magnesium alloys [5], and 42CrMo steel [6]. However, the above mentioned studies have neglected the influence of stress triaxiality on ductile fracture. In this respect, Benzerga et al. [7] discussed the widely used models of ductile fracture and pointed that the void volume fraction changes differently

under high and low stress triaxiality. Duan et al. [8, 9] discussed the influence of stress state and stress triaxiality on fracture strain and critical damage value of 316LN steel. Oyane [10, 11] proposed a ductile fracture criterion, considering stress triaxiality and plastic deformation capacity, which has become one of the most common criteria for cracking prediction in plastic forming. The use of Oyane ductile fracture criterion by Reddy et al. [12] and Lei et al. [13] enabled them to predict the crack initiation by numerical simulation, and the simulation results were in good agreement with experimental ones. However, Oyane criterion was only suitable for predicting cracks in cold forming and failed to consider the effects of strain rate and deformation temperature. Based on Oyane criterion, He et al. established ductile fracture criteria at elevated temperature for 30Cr2Ni4-MoV ultra-super-critical rotor steel [4], SA508-3 steel [14], 316LN stainless steel [15], and no. 50 steel [16], successfully anticipating the initiation and location of cracks by numerical simulation. Zhan et al. [17] proposed a thermal damage model for Ti-6Al-2Zr-1Mo-1V titanium alloy by combining the Oyane ductile fracture criterion with the damage threshold, temperature, and strain rate, successfully anticipating that the inner surface of the spinning region is the zone most prone to damage in the tube rolling-spinning.

To predict the occurrence of cracks in the casting-rolling compound forming process of ring parts, many scholars have studied the process and simulation of ring rolling deeply. For instance, Wu et al. performed a comprehensive and systematic study on the casting-rolling compound forming process of rings, reporting the influence of casting solidification parameters on the secondary dendrite arm spacing and crack defects [18], developing the method of grain refining during the solidification process [19], describing the metadynamic recrystallization [20], flow stress behavior upon hot deformation [21], and thermal physical properties of the as-cast 42CrMo steel [22], and establishing a hot working diagram of the as-cast 42CrMo steel [23]. The aforementioned results lay the foundation for the analysis of crack initiation in the casting-rolling compound forming process. However, no ductile fracture criteria for as-cast 42CrMo steel that would allow one to predict the emergence of cracks in the casting-rolling compound forming process of ring parts have been formulated until now.

In this paper, the model of critical fracture strain was first established for as-cast 42CrMo steel based on the tensile tests at different temperatures and strain rates. Besides, combining this model with Oyane criterion enabled one to obtain the ductile fracture criteria for 42CrMo steel at elevated temperature. The parameters of the proposed criterion were determined through experiments and numerical simulations. Based on DEFORM software platform, a FE model for fracture prediction of as-cast 42CrMo steel in hot ring rolling was first established. The evolution laws and mechanisms of damage and fracture in the process were revealed, which has an important role to play for the improvement of forming quality of 42CrMo steel ring.

2. Material and Methods of High-Temperature Tensile Experiments

The 42CrMo steel with a chemical composition given in Table 1 was cast according to the procedure described in [24]. The microstructure of 42CrMo as-cast ingots mainly consists of ferrite and pearlite, shown in Figure 1. The tensile specimens were designed according to GB6397-86 and machined, as shown in Figure 2(a).

The high-temperature tensile tests were carried out using the Gleeble-3500D thermomechanical simulator at various temperatures (1223, 1273, 1373, 1423, and 1473 K) and strain rates (0.001, 0.01, 0.1, and 1.0 s^{-1}). Prior to the experiments, the specimens were heated to 1473 K at a heating rate of 283 K/s. The temperature was maintained for 2 min to preserve heat and then dropped to deformation temperatures at a rate of 293 K/s. In order to avoid oxidation during tensile experiments, the specimens were kept in a vacuum. After tensile test, specimens were cooled by water immediately. The half part of broken specimen after high-temperature tensile test is shown in Figure 2(b).

The specimens were wire cut along their longitudinal axis. The sections were ground, polished, cleaned with alcohol, and finally etched for 140 s using picric acid-saturated water solution at the temperature 348 K. The microstructure of the fracture surface for tensile specimens was characterized using an optical microscope (OM).

3. Results and Discussion

3.1. Stress-Strain Curves. The true stress-strain curves of 42CrMo steel in tensile experiments under various temperatures and strain rates are shown in Figure 3. In Figure 3, the stress is very sensitive to strain rate and temperature. The peak stress σ_p and the corresponding strain ε_p increase with the rise of strain rate and decrease with increasing temperature. The thermal deformation curves of as-cast 42CrMo steel are divided into two categories as follows.

(1) Curves with a significant peak: during the initial stages of high-temperature tensile deformation, work hardening dominates and the stress-strain behaviors show a rapid increase in stress with increasing work hardening. With the increase of strain, dynamic recovery and recrystallization play a softening role, and the increase rate of flow stress slows down. Then, the stress reaches a maximum, after which the softening effect is dominant, the tensile specimen breaks, and the stress decreases [25, 26].

(2) Curves with no significant peak: when the specimens were tested at the high temperature and low strain rate (e.g., at 1423 K or 1473 K and 0.001 s^{-1}), work hardening dominates and stress values increase rapidly during the initial stages. The stress peak is not significant, and the deformation behavior is characterized by slightly strain hardening and approximately steady-state flow [27].

TABLE 1: Chemical composition of 42CrMo steel (wt%).

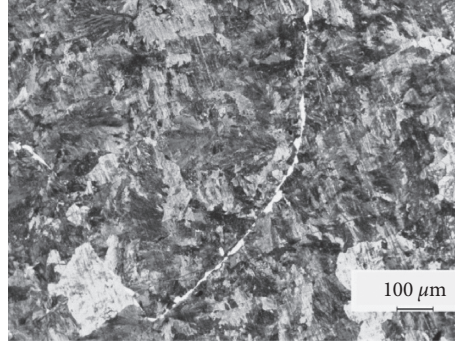| C	Si	Mn	Cr	Mo	P	S	Cu
0.4	0.23	0.6	0.98	0.18	0.019	0.012	0.02

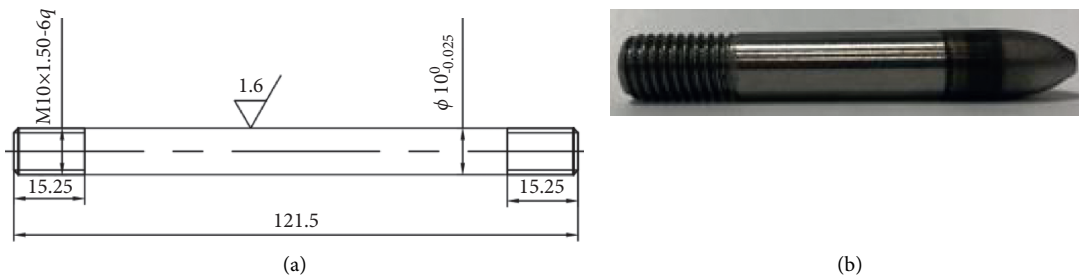FIGURE 1: Initial microstructure of as-cast 42CrMo.

(a)

(b)

FIGURE 2: (a) Dimensions of tensile specimen of as-cast 42CrMo steel. (b) Specimen after tensile tests.

3.2. Fracture Morphology. Microstructures in longitudinal section of the fracture surface for tensile specimens deformed at the strain rate $1 \, s^{-1}$ are shown in Figure 4. As can be seen from Figure 4, dynamic recrystallization occurs at the fracture surface of the tensile specimens. Many voids of different shapes and sizes can be seen at the fracture surface, and macroscopic fracture occurs when the voids grow and converge. Ductile fracture originates from cavity evolution and the driving force of cavity evolution is the stress concentration in the material [28]. The stress concentration at the contact position between the inclusion and the matrix causes the inclusion to fall off or break up from the matrix, and then the void nucleates. The newly formed voids and the initial voids in the material grow up and coalesce during deformation and finally form macroscopic fracture. The thermal deformation and dynamic recrystallization soften the material, relieve the stress concentration in the material, hinder the cavity growth, and change the cavity evolution and the fracture behavior of the material [29].

Therefore, with the increasing of temperature, the volume fraction of the dynamic recrystallized grains increases, larger areas of the cavity are obstructed from growth, and fracture toughness increases. Once the temperature exceeds some certain limit, grain is seriously coarsened, and the grain boundary turns to be weak, the microcracks may be easy to occur on the grain boundary, and fracture toughness severely decreases (shown in Figure 4(e)).

4. Determination and Analysis of Critical Fracture Strain

The critical fracture strain ε_f is the strain arising at the moment of necking [16]. It is an important parameter of ductile fracture, which can reflect the plastic deformation capacity [15, 16]. However, because of the high-temperature softening, critical fracture strain ε_f is difficult to be measured directly, especially at high temperatures and low strain rates. In present study, the technique described in [30, 31] is used for this purpose, which consists in converting the nonuniform deformation zone after necking into an equivalent zone with uniform deformation. This enabled one to obtain the critical fracture strains at different temperatures and strain rates (see the plots in Figure 5(a)).

At the constant strain rate, the critical fracture strain increases and then drops with the increase of deformation temperature. This is consistent with the physical mechanism of thermal forming and can be explained as follows.

The driving force for ductile fracture is the stress concentration within the material. With the increase of temperature, the atomic diffusions and grain boundary
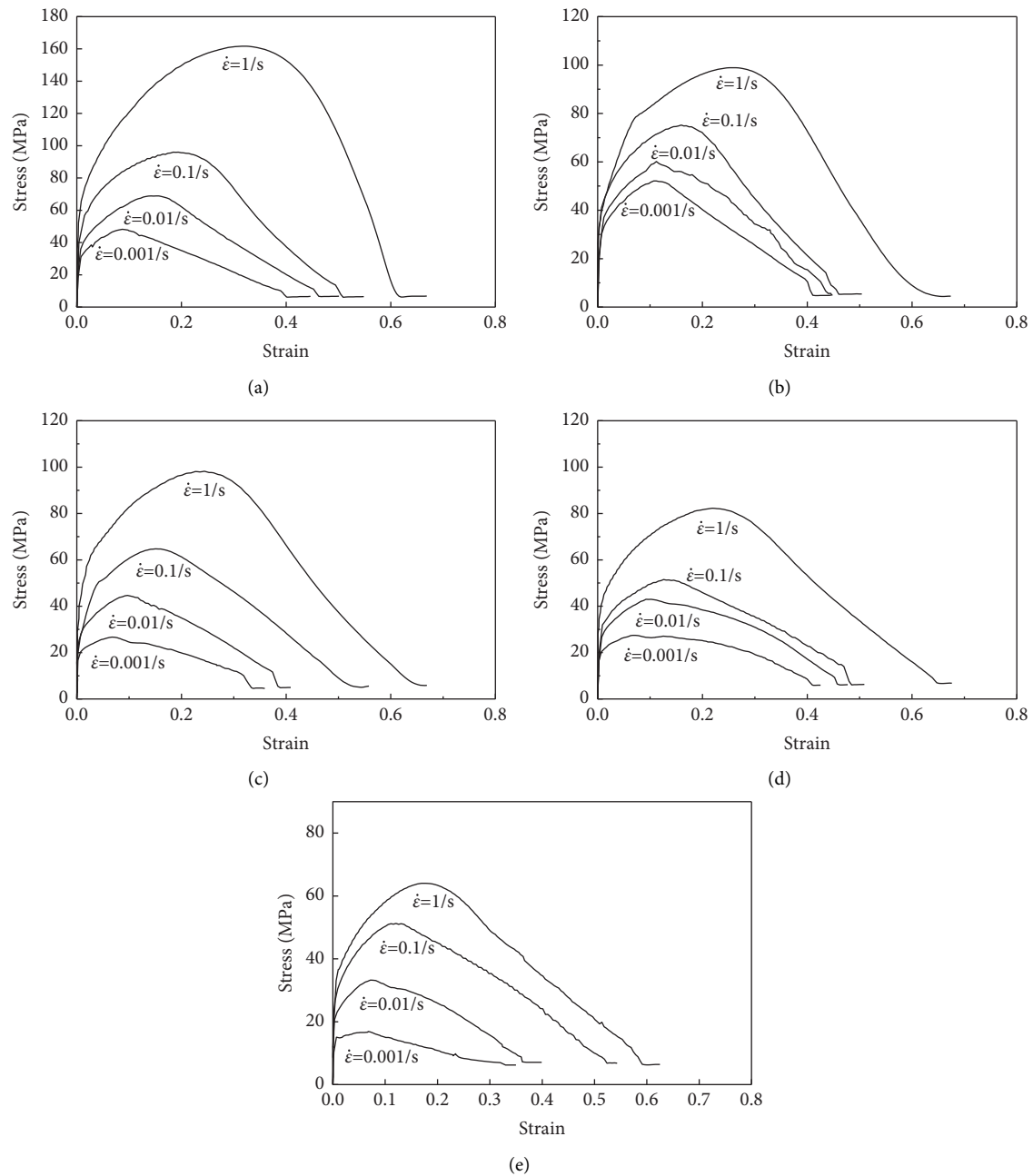
(a)

(b)

(c)

(d)

(e)

FIGURE 3: Relationships between true stress-strain for as-cast 42CrMo steel at different temperatures: (a) 1223 K. (b) 1273 K. (c) 1373 K. (d) 1423 K. (e) 1473 K.

migration become faster, enhancing the dynamic recrystallization and triggering the glide and climb of dislocations at reducing their density. This alleviates the stress concentration in the material and increases the critical fracture strain [32–34]. As the deformation temperature continues to increase to 1423 K (a critical temperature), the critical fracture strain reaches the peak value (see Figure 5(a)). The grain boundaries start to become weak and microcracks tend to occur at the grain boundaries. When the deformation temperature increases to 1473 K, the grains coarsen to a large extent, the grain

boundary turns to be weak, the microcracks is easy to occur on the grain boundary, and the critical fracture strain decreases.

At the constant deformation temperature, the critical fracture strain increases with the decrease of strain rate. At low strain rates, there is a sufficient time for atomic diffusions and grain boundary migration, resulting in the accelerated dynamic recrystallization. This reduces the dislocation density, alleviates the stress concentration in the material and, consequently, increases the critical fracture strain.
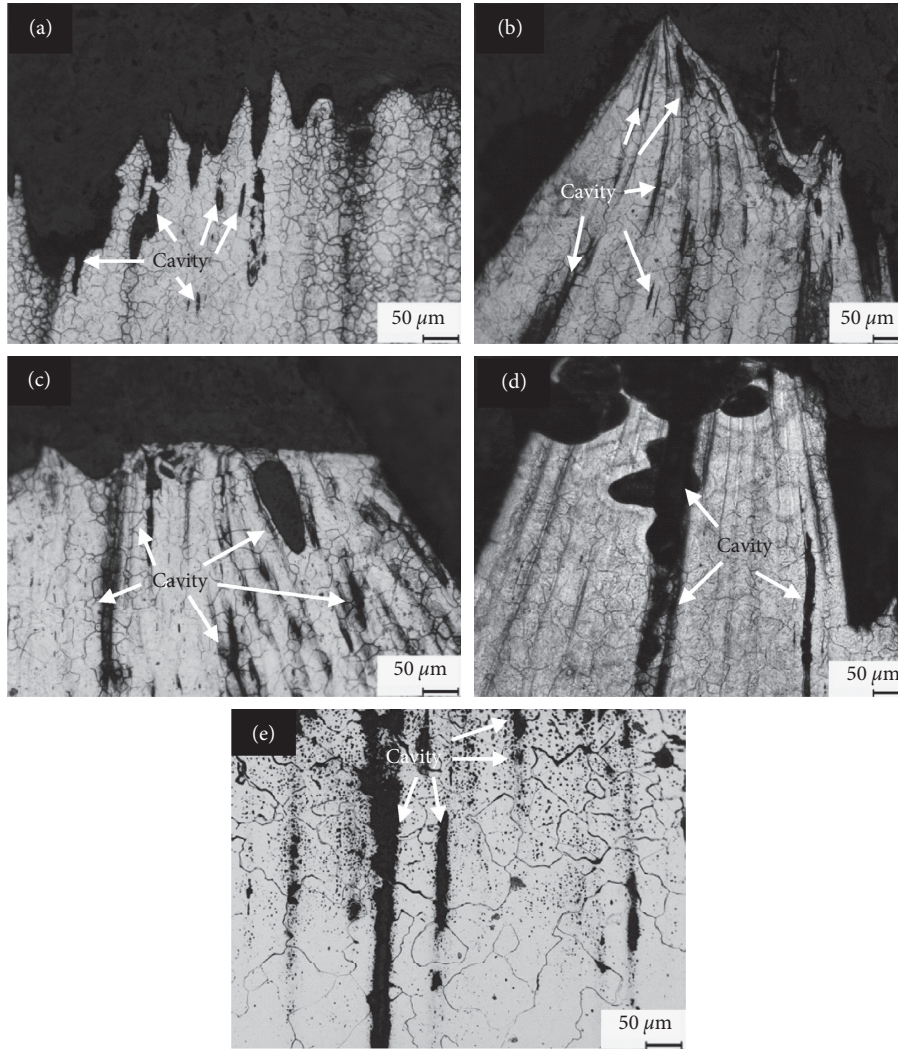
FIGURE 4: Microstructure in longitudinal section of fracture surface for sections at 1 s^{-1}: (a) 1223 K. (b) 1273 K. (c) 1373 K. (d) 1423 K. (e) 1473 K.

5. Establishment of a Model of Critical Fracture Strain

A thorough analysis of the parameter ε_f revealed its sensitivity to temperature and strain rate under hot deformation conditions. This finding allows the critical fracture strains ε_f to be expressed as a function [4] of temperature and strain rate:

$$\varepsilon_f = M\dot{\varepsilon}^a \cdot \left[\exp\left(\left| \frac{1}{T} - \frac{1}{T_c} \right| \cdot \frac{Q}{R} \right) \right]^b,$$ (1)

where Q is the thermal activation energy; R is the universal gas constant (8.31 J·mol^{-1}·K^{-1}); M, a, and b are the material parameters; and T_c is the critical temperature that can be assessed from Figure 4 by taking the average of all the critical temperatures at different strain rates ($T_c = 1423$ K). Among these, the parameters Q, M, a, and b are determined as follows.

5.1. Determination of Parameter Q. According to the data reported in [14–16, 35, 36] in conjunction with Arrhenius function [37], the thermal activation energy Q of as-cast 42CrMo steel can be expressed as

$$Q = R\left[\frac{\partial \ln \dot{\varepsilon}}{\partial \ln \ \sinh(\alpha\sigma)} \right]_T \left[\frac{\partial \ln \ \sinh(\alpha\sigma)}{\partial (1/T)} \right]_{\dot{\varepsilon}},$$ (2)

and its value is found to be $Q = 241.175$ kJ·mol^{-1}.

5.2. Determination of Parameter a. Keeping T constant, equation (1) can be rewritten as

$$a = \frac{\partial \ln \ \varepsilon_f}{\partial \ln \dot{\varepsilon}},$$ (3)
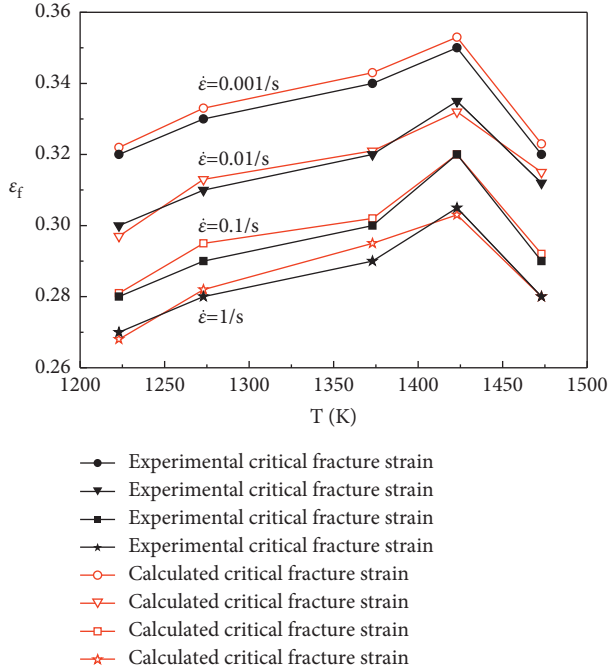
resulting in $a = -0.028$.

FIGURE 5: Critical fracture strains at different temperatures and strain rates for as-cast 42CrMo steel. (a) Experimental critical fracture strain. (b) Calculated critical fracture strain.

5.3. Determination of Parameter b. Keeping $\dot{\varepsilon}$ constant, equation (1) can be redefined as

$$b = \frac{\partial \ln \varepsilon_f}{\partial \left(-\left|(1/T) - (1/T_c)\right|(Q/R),\right.} \tag{4}$$

and it is evaluated as $b = 0.0462$.

5.4. Determination of Parameter M. By substituting the parameters $Q = 241.175$ kJ·mol^{-1}, $R = 8.31$ J·mol^{-1}·K^{-1}, $a = -0.028$, $b = 0.0462$, and $T_c = 1423$ K in equation (1), the value of M can be gained by applying the inverse calculation and $M = 0.3$ is obtained.

Thus, by substituting the parameters Q, R, a, b, T_c, and M into equation (1), the model of critical fracture strain is expressed as

$$\varepsilon_f(T, \dot{\varepsilon}) = 0.3\dot{\varepsilon}^{-0.028} \cdot \left[\exp\left(-29022 \cdot \left|\frac{1}{T} - \frac{1}{1423}\right|\right)\right]^{0.0462}. \tag{5}$$

The calculated values of ε_f calculated by equation (5) are shown in Figure 5(b). The comparison between the calculated critical fracture strain and experimental results is shown in Figure 6. It is found that the calculated results are in good agreement with experimental results. The correlation coefficient is 0.9925, and the average relative deviation is 1.20%.

6. Establishment of Thermal Ductile Fracture Criterion

The ductile fracture criterion is the critical condition that allows one to quantitatively describe the critical fracture
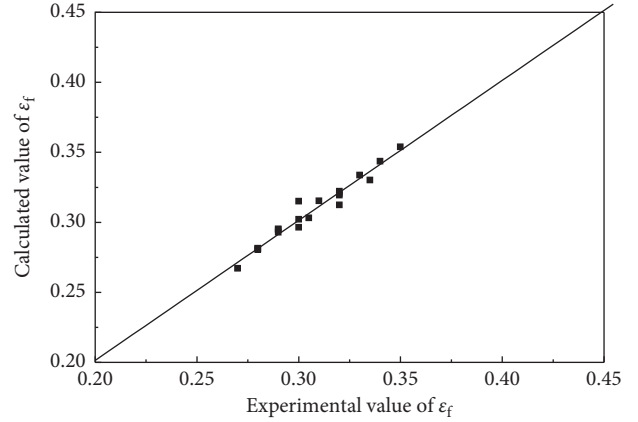

FIGURE 6: Comparison of the calculated critical fracture strain ε_f with experimental results.

occurrence during the forming. In particular, Oyane criterion is one of the widely used criteria in cold forming [10, 11, 38]. Many researchers pointed out the reliable prediction ability of Oyane criterion [39–41] and the others pointed out its robustness [42–46]. Oyane criterion well describes the impact of stress triaxiality on fracture while failing to consider the effects of strain rate and temperature. However, ductile fracture is a complex phenomenon depending on various process parameters including stress states, strain, strain rate, and forming temperature. Thus, the strain rate and temperature should be taken into consideration when defining the reliable fracture criterion for as-cast 42CrMo steel at elevated temperature.

Given the previously mentioned influence factors and based on Oyane criterion, the ductile fracture criterion for as-cast 42CrMo steel at elevated temperature can be established as follows:

$$D = \frac{C}{C_f} = \frac{\int_0^{\overline{\varepsilon}_f} \left(1 + (\sigma_m/B\overline{\sigma})\right)d\overline{\varepsilon}}{C_f(\dot{\varepsilon}, T)} \geq 1, \tag{6}$$

where D is the damage ratio, C is the cumulative fracture damage value under different stress states, C_f is the critical damage threshold of fracture failure, C_f is a variate affected by temperatures and strain rates during hot forming, and $\sigma_m/\overline{\sigma}$ is the stress triaxiality.

In the uniaxial tension test, C_f can be expressed as

$$C_f(\dot{\varepsilon}, T) \geq \left(1 + \frac{1}{3B}\right)\varepsilon_f. \tag{7}$$

Substituting equation (5) into equation (7) results in

$$C_f(\dot{\varepsilon}, T) \geq \left(1 + \frac{1}{3B}\right)0.3\dot{\varepsilon}^{-0.028} \cdot \left[\exp\left(-29022 \cdot \left|\frac{1}{T} - \frac{1}{1423}\right|\right)\right]^{0.0462}. \tag{8}$$

Substituting equation (6) into equation (8) results in

$$\int_0^{\overline{\varepsilon}_f} \left(1 + \frac{\sigma_m}{B\overline{\sigma}}\right) d\overline{\varepsilon} \geq \left(1 + \frac{1}{3B}\right) \cdot 0.3\dot{\varepsilon}^{-0.028} \cdot \left[\exp\left(-29022 \cdot \left|\frac{1}{T} - \frac{1}{1423}\right|\right)\right]^{0.0462}. \tag{9}$$

Equation (9) is the critical condition for the occurrence of instantaneous fracture. However, as the temperature and strain rate vary in the course of hot deformation, this process can be divided into many time steps. In each time step, the temperature and strain rate are assumed to be constant, and

the cumulative damage value is the accumulation of damage of each incremental step during the whole hot deformation process. Then, the ductile fracture criterion under arbitrary stress can be determined as

$$D = \frac{C}{C_f} = \frac{\sum_{i=1}^{N} \left(1 + \left(\sigma_{mi}(\dot{\varepsilon}_i, T_i)/B\overline{\sigma}(\dot{\varepsilon}_i, T_i)\right)\right) \cdot \Delta\varepsilon_i}{(1 + (1/3B)) \cdot 0.3\dot{\varepsilon}^{-0.028} \cdot \left[\exp\left(-29022 \cdot |(1/T) - (1/1423)|\right)\right]^{0.0462}} \geq 1, \tag{10}$$

where i is the index of time step; N is the total amount of time steps; B is the stress compensation factor which is a constant. When the cumulative damage value C is greater than (or equal to) the critical damage threshold C_f, that is, the damage ratio $D \geq 1$, the cracks occur.

It is noteworthy that how to determine the material constant B accurately is the key problem to establish the criterion equation. Some scholars [40, 47, 48] pointed out that the stress state during the deformation could exert influence on the deformation patterns and affect crack evolution. An effective solution for this problem was proposed by He et al. [4] who implemented the upsetting tests

with different stress triaxialities in conjunction with FE simulations to obtain the parameter B.

The dimensions of upsetting test samples are listed in Table 2. The cylindrical upsetting (CUP-20), tapered upsetting (TUP-30), and double-cone upsetting (DUP-36) with the same ratio of height and diameter were performed on a hydraulic press at the stroking speed of 5.0 mm/s and the temperature of 1373 K. Finally, applying the least square fit method to the results enabled one to obtain $B = 0.267$.

Substituting the value B into equation (10), the ductile fracture criterion of as-cast 42CrMo steel at elevated temperature can be expressed as

$$D = \frac{C}{C_f} = \frac{\sum_{i=1}^{N} \left(1 + \left(\sigma_{mi}(\dot{\varepsilon}_i, T_i)/0.267 \cdot \overline{\sigma}(\dot{\varepsilon}_i, T_i)\right)\right) \cdot \Delta\varepsilon_i}{0.6745\dot{\varepsilon}^{-0.028} \cdot \left[\exp\left(-29022 \cdot |(1/T) - (1/1423)|\right)\right]^{0.0462}} \geq 1. \tag{11}$$

According to equation (11), it can be seen that the damage value C increases with increasing stress triaxiality and plastic strain, and the critical damage threshold C_f decreases with the decrease in temperature T and the increase in strain rate $\dot{\varepsilon}$. Therefore, low deformation temperature and high strain rate are beneficial to the emergence of cracks in the steel while exposed to hot ring rolling.

7. Verification of Ductile Fracture Criterion

In order to validate the reliability of the established ductile fracture criterion for as-cast 42CrMo steel, the FE simulations of tensile and upsetting tests were performed to compare with corresponding experimental results. Before the FE simulations, the developed fracture criterion equation (11) was embedded into the postprocessor by user subroutine in DEFORM platform. The adaptive meshing technology was used to reduce element distortion. The constitutive model of material was adopted the same as the stress-strain curves in Figure 3. Thermal-physical characteristic parameters of as-cast 42CrMo steel were from [22].
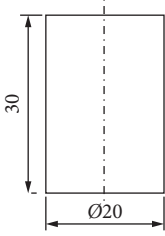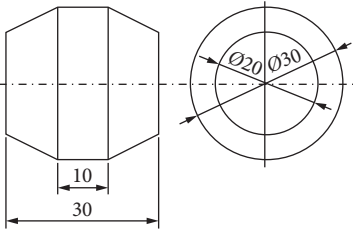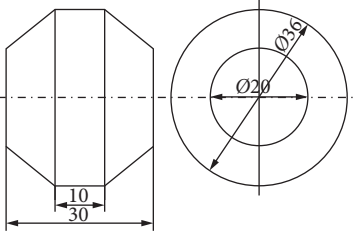
7.1. Simulation of Tensile Tests. The dimensions of tensile specimen in simulation are the same as that in tensile test.

Because the specimen is symmetric, the half was modeled with symmetry constraint. The middle part of the necked sample was partially refined by the mesh and partially heated at high temperature.

The simulation results of the corresponding tensile tests at 1373 K and 0.1 s^{-1} are shown in Figure 7. It can be seen that cracks initiate and propagate from the center of the necked specimen and cracks occur when the damage ratio is equal to or above 1. The tensile fracture morphology obtained by scanning electron microscopy (SEM) is shown in Figure 8. It can be seen from Figure 8 that cracks initiate and propagate from the center of the necked specimen. Simulation results are found to coincide with the images in Figure 8, revealing the same behavior of cracks. Thus, the established ductile fracture criterion enables one to accurately predict the occurrence and location of cracks for as-cast 42CrMo steel in high temperature deformation.

7.2. Simulation of Upsetting Tests. The dimensions of upsetting specimens and boundary loading condition in simulation are the same as those in upsetting tests. The movement speed of upper mold was set to 5.0 mm/s. Friction coefficient was set to 0.3. The simulation results of the

TABLE 2: As-cast 42CrMo steel specimens with different geometric shapes and sizes.

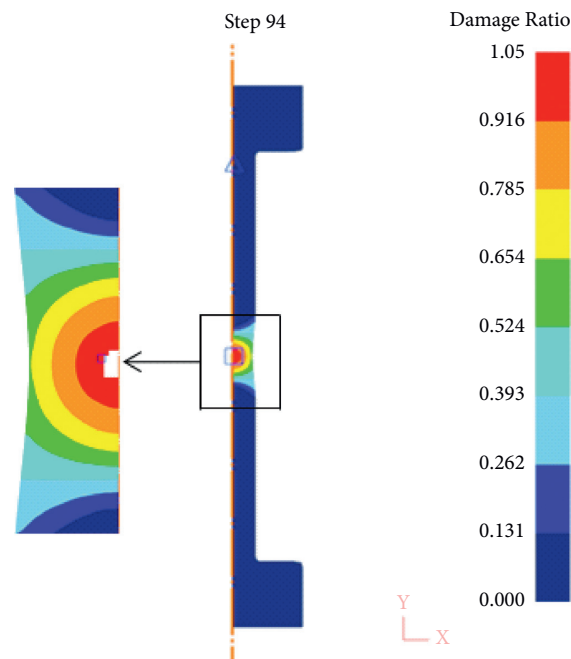| Cylinder (CUP-20, $H/D = 1.5$)	Taper (TUP-30, $H/D = 1.5$)	Double-cone (TUP-36, $H/D = 1.5$)

FIGURE 7: Schematic diagrams of the rupture location based on the numerical simulation using the developed ductile fracture criterion for as-cast 42CrMo steel at 1373 K and 0.1 s^{-1}.
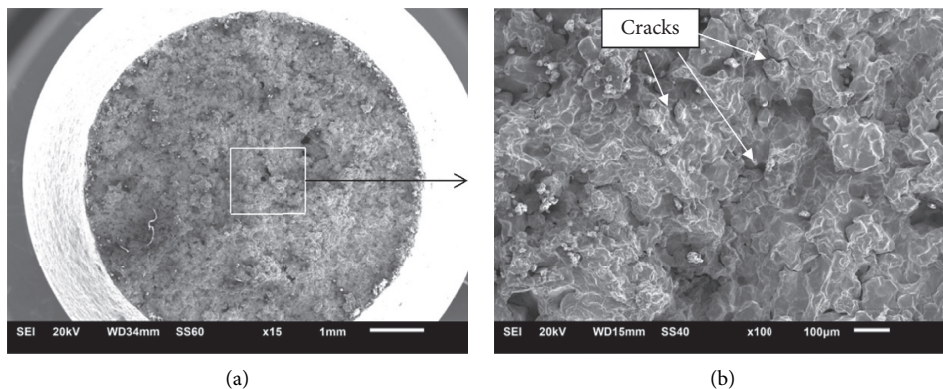

(a)   (b)

FIGURE 8: SEM fracture morphology in the central region of a tensile specimen deformed at 1373 K and 0.1 s^{-1}. (a) General view. (b) Highlighted area of the white box.

corresponding upsetting tests at 1373 K are shown in Figure 9. It can be seen that cracks initiate at the equatorial free surface of the upsetting specimens at their critical height reduction ratios of 61.8% (CUP-20), 53.3% (TUP-30), and 50.3% (DUP-36), respectively. Rupture phenomenon after the upsetting tests is shown in Figure 10. It can be seen that cracks also initiate at the equatorial free surface in upsetting tests, and the margin of critical height reduction ratios error
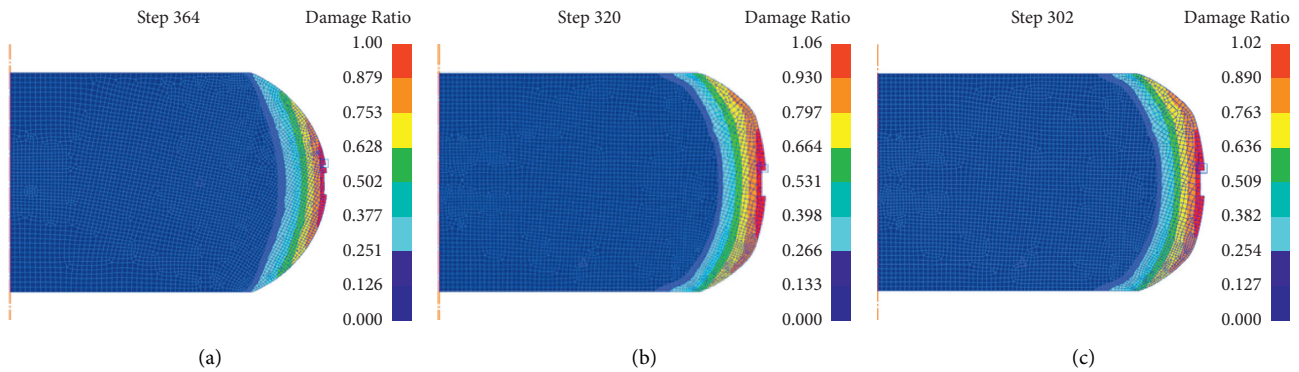
FIGURE 9: Occurrence of cracks at 1373 K and the stroking speed of 5 mm/s for the critical height reduction ratios of (a) 61.8% (CUP-20), (b) 53.3% (TUP-30), and (c) 50.3% (TUP-36).
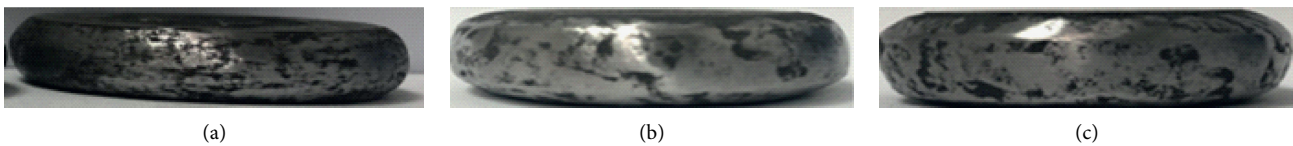

FIGURE 10: Rupture phenomenon after the upsetting tests at 1373 K and the stroking speed of 5 mm/s for the critical height reduction ratios of (a) 65.7% (CUP-20), (b) 52.3% (TUP-30), and (c) 51.4% (TUP-36).

between simulation and upsetting tests is about three percentage points. The simulation data (see Figure 9) are in good agreement with experimental results (see Figure 10), evidencing the reliability of the established ductile fracture criterion for prediction of the occurrence and location.

8. Application of Ductile Fracture Criterion in Hot Ring Rolling

8.1. Establishment of the FE Model Coupled with Damage for Ring Rolling. Process parameters used in simulation are shown in Table 3. The motion control over guide rolls was realized by inputting the model of motion control [49] into DEFORM-3D platform. Friction coefficient [50] was set to 0.7. The constitutive model and thermal-physical characteristic parameters of as-cast 42CrMo steel are the same as Section 6. The FE model for ring rolling of as-cast 42CrMo was established, as shown in Figure 11.

8.2. Mechanism of Damage and Fracture during the Hot Ring Rolling Process

8.2.1. The Evolution Laws of Damage Value and Stress Triaxiality. Damage value C distribution can be derived from simulation results of hot ring rolling, as shown in Figure 12. It can be seen from Figure 12 that the damage value C is large at the top and bottom edges of the inner surface area of the ring, while the damage value C is least in the central section of inner surface area of the ring. The reason of evolution law of damage value can be explained as follows.

Stress triaxiality distribution can be derived from simulation results of hot ring rolling, as shown in Figure 13. As shown in Figure 13, the stress triaxiality is negative in most areas of the ring under the extrusion force of the rolls, and positive stress triaxiality only appears near the top and bottom edges of the inner and outer surface areas. In order to further explore the evolution laws of stress triaxiality and damage value, three particular nodes shown in Figure 14 were selected for tracking. The evolution laws of stress triaxiality and damage value for the particular nodes in the region are visualized in Figures 15(a) and 15(b). It can be seen that there is a periodic sequence phenomenon of negative and positive stress triaxiality, which is due to the periodic rolling of the rollers on the material. The positive stress triaxiality accelerates the accumulation of damage value, while the negative stress triaxiality slows down the accumulation of damage value to a large extent. Therefore, with the increase of plastic strain in the hot ring rolling, the damage mainly accumulates at the top and bottom edges of the inner and outer surface areas. Because the plastic strain of the inner surface is greater than that of the outer surface, a larger accumulated damage value is located at the top and bottom edges of the inner surface area of the ring.

8.2.2. The Evolution Law of Damage Ratio. Using the FE model for hot ring rolling, the distribution law of the damage ratio was derived as shown in Figure 16. It can be seen that the large damage ratio, leading to cracking, is located at the top and bottom edges of the drive roll contact area. The reason can be explained as follows.

The damage value C is large at the top and bottom edges of inner surface areas. Moreover, at the top and bottom

TABLE 3: Process parameters used in simulation.

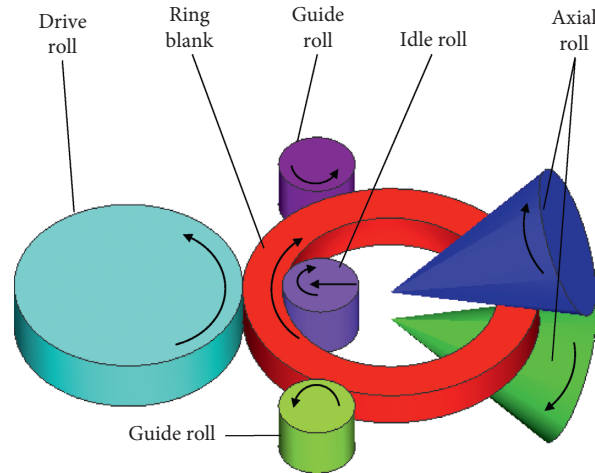| Parameter	Value
Dimension of casting ring blank (mm × mm × mm)	$864 \times 530 \times 234$
Radius of drive roll R_1 (mm)	450
Radius of idle roll R_2 (mm)	140
Radius of guide roll R_3 (mm)	140
Ambient temperature T (K)	293
Rotation speed of drive roll n_1 (r·m^{-1})	29.2
Feed rate of idle roll (mm·s^{-1})	6.4
Modulus of elasticity E (MPa)	119028
Poisson's ratio μ	0.35
Initial rolling temperature T (K)	1373

FIGURE 11: The finite element model of the hot ring rolling process.
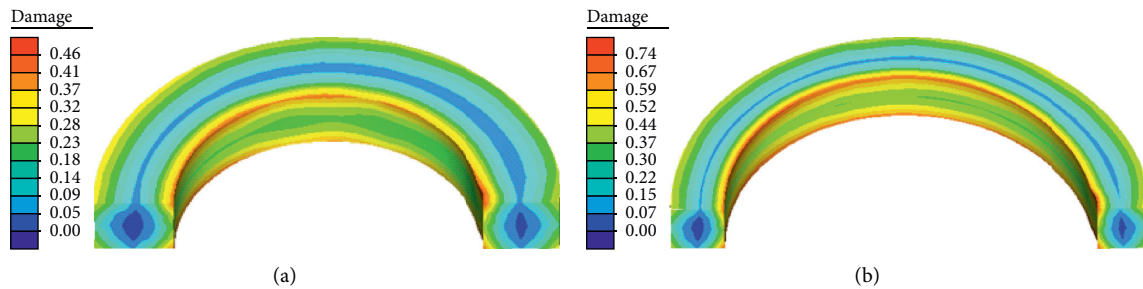
FIGURE 12: Damage value C distribution in hot ring rolling. (a) In the middle. (b) At the end of the process.

edges of inner surface area, the temperature is lower, and the strain rate is larger than that in other areas of ring. Therefore, the damage threshold C_f is small and damage ratio D is large at the corresponding areas. From Figure 16(b), it can be seen that the damage ratio D reaches 1.04, which shows that there is cracking at the top and bottom edges of inner surface area of the ring.

8.2.3. The Application of Ductile Fracture Criterion in Hot Ring Rolling. The parameters in the hot rolling experiment have been kept consistent with those in FE

simulation. Hot ring rolling experiment is shown in Figure 17(a). Cracking of the ring in the hot ring rolling experiment is shown in Figure 17(b). It can be seen that cracks of the ring in experiment appear at the top edge of inner surface. The thickness reduction in the hot rolling experiment is 58%, which is near to that in the FE simulation. The experimental result in Figure 17(b) is consistent with simulation result in Figure 16(b), therefore verifying the reliability of the criterion further and allowing the proposed ductile fracture criterion to be used for the prediction of cracks in the course of the ring rolling process.
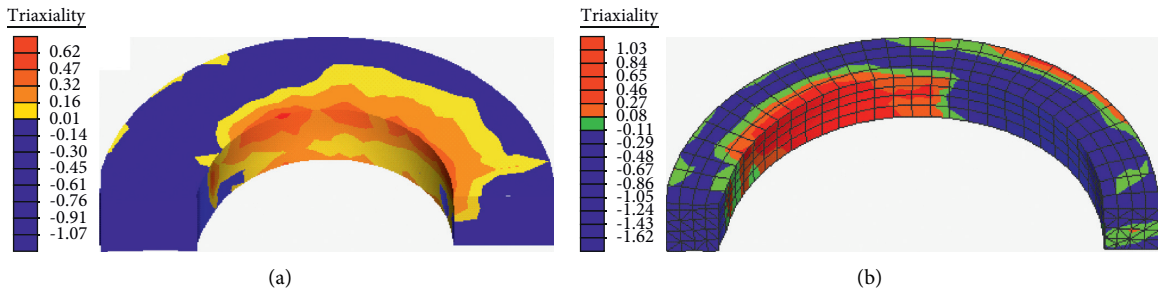
Figure 13: Stress triaxiality distribution in hot ring rolling. (a) In the middle. (b) At the end of the process.
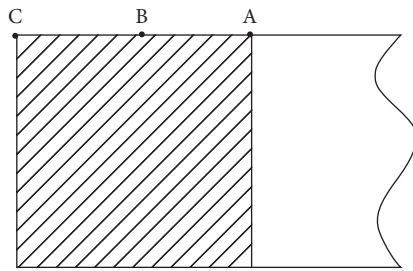

Figure 14: Selection of particular nodes.
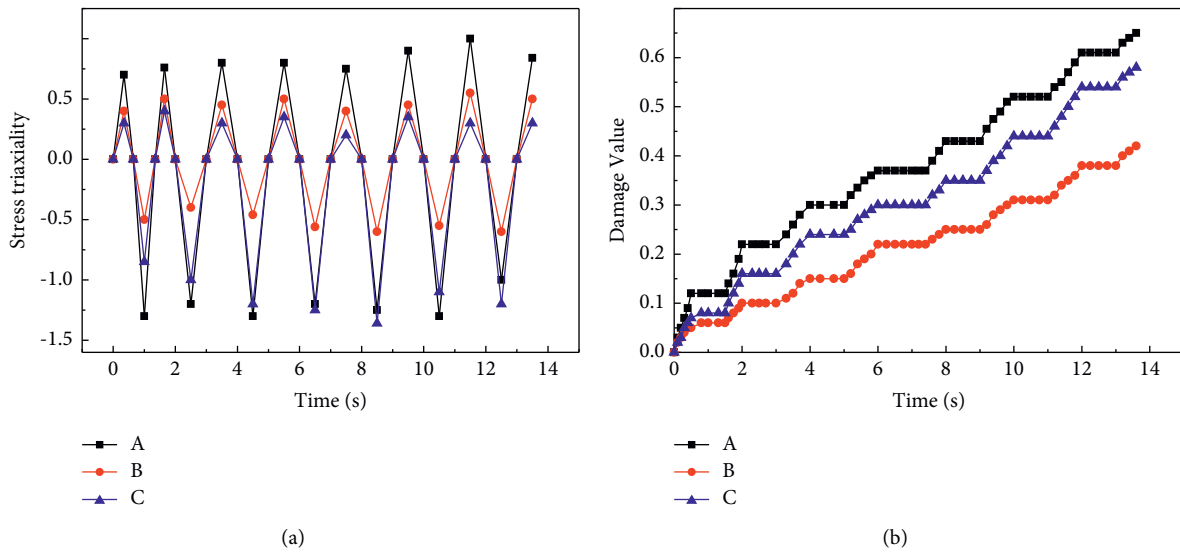

Figure 15: Evolutions of variables for the particular nodes in hot ring rolling. (a) Stress triaxiality. (b) Damage value.
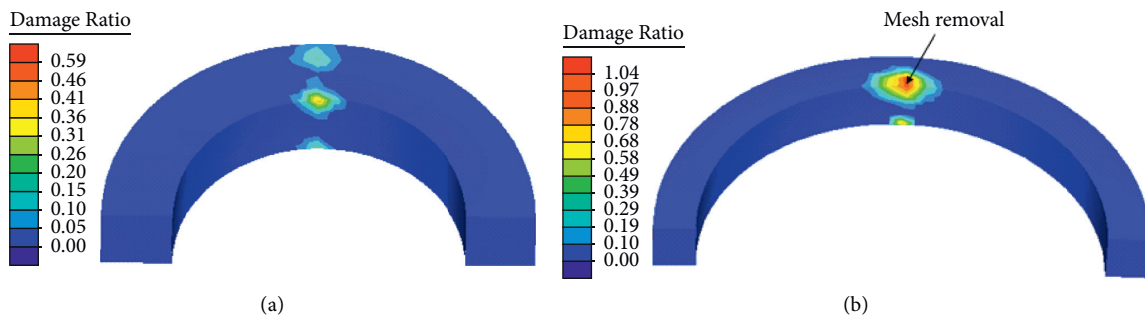

Figure 16: Damage ratio D distribution in hot ring rolling. (a) In the middle. (b) At the end of the process.

(a)   (b)

FIGURE 17: Cracking of ring in the hot ring rolling experiment. (a) Hot ring rolling experiment. (b) Cracking of the ring.

9. Conclusions

(1) The tensile fracture behavior of as-cast 42CrMo steel at elevated temperature was studied, revealing the sensitivity of the critical fracture strain to deformation temperature and strain rate. The model of critical fracture strain as a function of temperature and strain rate was established.

(2) With the increasing of temperature, dynamic recrystallization increases, the cavity are obstructed from growth, and fracture toughness increases. However, when the temperature reaches 1473 K, the microcracks may be easy to occur on the grain boundary, and fracture toughness decreases.

(3) The ductile fracture criterion for as-cast 42CrMo steel at elevated temperature was established. The proposed criterion was shown to be valid for the prediction of occurrence and location of cracks in the specimens exposed to tensile and upsetting tests.

(4) Positive stress triaxiality appears near the top and bottom edges of the inner surface area of the ring and accelerates the accumulation of damage value. These two effects make the damage value C large at the top and bottom edges of the inner surface area of the ring.

(5) The damage threshold C_f is small in the zone. Therefore, the damage ratio D is large at the top and bottom edges of the inner surface area of the ring, which have the greatest propensity to cracking in the course of hot ring rolling. This is consistent with the phenomenon of cracking in hot ring rolling experiment, allowing the proposed ductile fracture criterion to be used for the prediction of cracks at the elevated temperatures.

Data Availability

The data used to support the findings of this study are available from the corresponding author upon request.

Conflicts of Interest

The authors declare that there are no conflicts of interest.

Acknowledgments

References

[1] X. W. Duan, X. Z. Zhang, X. P. Wei, J. S. Liu, W. W. He, and J. H. Tian, "Application of ductile fracture criterion in hot forging damage of Mn18Cr18N steel," *Advanced Materials Research*, vol. 139-141, no. 141, pp. 510–515, 2010.

[2] Y. F. Xia, G. C. Luo, and D. S. Wu, G.-Z. Quan and J. Zhou, "The Evaluation of varying ductile fracture criteria for 3Cr20Ni10W2 austenitic heat resistant alloy," *Advances in Mechanical Engineering*, vol. 5, no. 3, pp. 1–10, 2013.

[3] X.-m. Zhang, W.-d. Zeng, Y. Shu et al., "Fracture criterion for predicting surface cracking of Ti40 alloy in hot forming processes," *Transactions of Nonferrous Metals Society of China*, vol. 19, no. 2, pp. 267–271, 2009.

[4] J. He, Z. Cui, F. Chen, Y. Xiao, and L. Ruan, "The new ductile fracture criterion for 30Cr2Ni4MoV ultra-super-critical rotor steel at elevated temperatures," *Materials & Design*, vol. 52, pp. 547–555, 2013.

[5] W. J. Kim, H. K. Kim, W. Y. Kim et al., "Temperature and strain rate effect incorporated failure criteria for sheet forming of magnesium alloys," *Materials Science and Engineering A*, vol. 488, no. 1, pp. 468–474, 2008.

[6] Y. C. Lin, Y.-X. Liu, G. Liu, M.-S. Chen, and Y.-C. Huang, "Prediction of ductile fracture behaviors for 42CrMo steel at elevated temperatures," *Journal of Materials Engineering and Performance*, vol. 24, no. 1, pp. 221–228, 2015.

[7] A. A. Benzerga, J.-B. Leblond, A. Needleman, and V. Tvergaard, "Ductile failure modeling," *International Journal of Fracture*, vol. 201, no. 1, pp. 29–80, 2016.

[8] X. W. Duan and J. S. Liu, "Influence of stress triaxiality on critical damage value of 316LN steel," *Journal of Plasticity Engineering*, vol. 21, no. 3, pp. 128–131, 2014.

[9] X. W. Duan and J. S. Liu, "Influence of stress state on Plasticity of 316LN steel at elevated Temperature," *Journal of Beijing University of Technology*, vol. 40, no. 3, pp. 460–465, 2014.

[10] M. Oyane, T. Sato, K. Okimoto, and S. Shima, "Criteria for ductile fracture and their applications," *Journal of Mechanical Working Technology*, vol. 4, no. 1, pp. 65–81, 1980.

[11] M. Oyane, "Criteria of ductile fracture strain," *Bulletin of JSME*, vol. 15, no. 90, pp. 1507–1513, 1972.

[12] N. V. Reddy, P. M. Dixit, and G. K. Lal, "Ductile fracture criteria and its prediction in axisymmetric drawing,"

International Journal of Machine Tools and Manufacture, vol. 40, no. 1, pp. 95–111, 2000.

[13] L.-P. Lei, J. Kim, and B.-S. Kang, "Bursting failure prediction in tube hydroforming processes by using rigid-plastic FEM combined with ductile fracture criterion," *International Journal of Mechanical Sciences*, vol. 44, no. 7, pp. 1411–1428, 2002.

[14] J. L. He, Y. H. Xiao, J. Liu, Z. S. Cui, and L. Q. Ruan, "Model for predicting ductile fracture of SA508-3 steel undergoing hot forming," *Materials Science and Technology*, vol. 30, no. 10, pp. 1239–1247, 2014.

[15] J.-l. He, J. Liu, Z.-s. Cui, C.-z. Yang, and F. Chen, "Ductile fracture prediction of 316LN stainless steel in hot deformation process," *Journal of Iron and Steel Research International*, vol. 21, no. 10, pp. 923–930, 2014.

[16] J. L. He, Y. H. Xiao, Z. S. Cui, and F. Chen, "A novel ductile criterion for hot forming and its applicability," *Journal of Shanghai Jiao Tong University*, vol. 47, no. 11, pp. 1707–1711, 2013.

[17] M. Zhan, T. Zhang, H. Yang, and L. J. Li, "Establishment of a thermal damage model for Ti-6Al-2Zr-1Mo-1V titanium alloy and its application in the tube rolling-spinning process," *International Journal of Advanced Manufacturing Technology*, vol. 87, no. 5-8, pp. 1345–1357, 2016.

[18] Y. Wu, Y. T. Li, and L. Jia, "Effect of cooling rate on secondary dendrite arm spacing and crack defects of 42CrMo casting," *Journal of Mechanical Engineering*, vol. 50, no. 16, pp. 104–111, 2014.

[19] H. Yan and Y. T. Li, "Study on the microstructure and mechanical properties of Q235B ring casting blank," *Journal of Mechanical Engineering*, vol. 50, no. 14, pp. 89–94, 2014.

[20] H. Qi and Y. Li, "Metadynamic recrystallization of the as-cast 42CrMo steel after normalizing and tempering during hot compression," *Chinese Journal of Mechanical Engineering*, vol. 25, no. 5, pp. 853–859, 2012.

[21] H. P. Qi, Y. T. Li, J. Fu, and Z. Q. Liu, "Flow stress behavior of the normalized and tempered as-cast 42CrMo steel during hot deformation," *Advanced Materials Research*, vol. 314-316, no. 316, pp. 2560–2564, 2011.

[22] Y. Li, Y. Qing, H. P. Qi, J. Li, H. Lin, and G. Lianggang, "Study on the thermal-physical characteristic parameters of casting 42CrMo based on cast-rolling forming technology," *Journal of Mechanical Engineering*, vol. 50, no. 16, pp. 77–82, 2014.

[23] H. Chen, J. X. Bai, H. P. Qi, F. Jianhua, and L. Yongtang, "Establishment of hot processing maps and hot ring rolling process of 42CrMo steel," *Journal of Mechanical Engineering*, vol. 50, no. 16, pp. 89–96, 2014.

[24] Y. Li, H. P. Qi, Q. S. Li, C. Guozhen, Z. Lei, and Q. Fangcheng, "Casting process and experimental research of 42CrMo ring blanks based on cast-rolling forming technology," *Journal of Mechanical Engineering*, vol. 49, no. 20, pp. 49–54, 2013.

[25] J. M. Feng, E. Giraud, X. D. Cao, S. H. Li, and D. S. Philippe, "Study on constitutive equations of 2024 aluminum alloy considering the compensation of strain," *Journal of Plasticity Engineering*, vol. 24, no. 6, pp. 151–156, 2017.

[26] M. Noda, H. Mori, and K. Funami, "Transition in deformation mechanism of AZ31 magnesium alloy during high-temperature tensile deformation," *Journal of Metallurgy*, vol. 2011, no. 11, 10 pages, Article ID 165307, 2011.

[27] X. Liu, R. Chen, and E. Han, "High temperature deformations of Mg-Y-Nd alloys fabricated by different routes," *Materials Science and Engineering A*, vol. 497, no. 1-2, pp. 326–332, 2008.

[28] E. Hug, M. Martinez, and J. Chottin, "Temperature and stress state influence on void evolution in a high-strength dual-phase steel," *Materials Science and Engineering A*, vol. 626, pp. 286–295, 2015.

[29] X. Shang, Z. Cui, and M. W. Fu, "Dynamic recrystallization based ductile fracture modeling in hot working of metallic materials," *International Journal of Plasticity*, vol. 95, pp. 105–122, 2017.

[30] J. L. He, "Research on ductile fracture criteria of structural steels used in nuclear and thermal power during hot forming at high temperature and in their applications," Doctor's thesis, Shanghai Jiao Tong University, Shanghai, China, 2014.

[31] C. Z. Yang, "Research on fracture and damage condition for 316LN steel during hot deformation," Master's thesis, Shanghai Jiao Tong University, Shanghai, China, 2014.

[32] P. L. Pan, "Research on the dynamic recrystallization behavior of 316LN steel under multi-pass deformation," *Journal of Plasticity Engineering*, vol. 18, no. 5, pp. 13–18, 2011.

[33] J. X. Zang, Z. H. Feng, X. F. Zhang, S.-L. Dai, and L.-X. Tao, "Influence of the deformation parameters on microstructures of a new Al-Zn-Mg-Cu high strength aluminum alloy," *Journal of Plasticity Engineering*, vol. 18, no. 5, pp. 38–42, 2011.

[34] X. L. Zhang, C. J. Zhuang, and L. K. Ji, "Effective particle size of high grade pipeline steel," *Materials for Mechanical Engineering*, vol. 20, no. 3, pp. 60–64, 2013.

[35] S. S. Bhattacharya, G. V. Satishnarayana, and K. A. Padmanabhan, "A generic analysis for high-temperature power-law deformation: the case of linear in (strain rate)-In(stress) relationship," *Journal of Materials Science*, vol. 30, no. 23, pp. 5850–5866, 1995.

[36] A. M. Brown and M. F. Ashby, "On the power-law creep equation," *Scripta Metallurgica*, vol. 14, no. 12, pp. 1297–1302, 1980.

[37] C. Zhang, X. Q. Li, D. S. Li, C.-hai Jin, and J. Xiao, "Modelization and comparison of Norton-Hoff and Arrhenius constitutive laws to predict hot tensile behavior of Ti-6Al-4V alloy," *Transactions of Nonferrous Metals Society of China*, vol. 22, no. 2, pp. S457–S464, 2012.

[38] P. Hora, L. Tong, B. Berisha, and C. Karadogan, "Damage dependent stress limit model for failure prediction in bulk forming processes," *International Journal of Material Forming*, vol. 4, no. 3, pp. 329–337, 2011.

[39] N. Bonora, A. Ruggiero, L. Esposito, and D. Gentile, "CDM modeling of ductile failure in ferritic steels: assessment of the geometry transferability of model parameters," *International Journal of Plasticity*, vol. 22, no. 11, pp. 2015–2047, 2006.

[40] B. P. P. A. Gouiveia, J. M. C. Rodrigues, and P. A. F. Martins, "Ductile fracture in metalworking: experimental and theoretical research," *Journal of Materials Processing Technology*, vol. 101, no. 1–3, pp. 52–63, 2000.

[41] P. Mcallen and P. Phelan, "A method for the prediction of ductile fracture by central bursts in axisymmetric extrusion," *ARCHIVE Proceedings of the Institution of Mechanical Engineers Part C Journal of Mechanical Engineering Science*, vol. 219, no. 3, pp. 237–250, 2005.

[42] J. Mackerle, "Finite element analyses and simulations of manufacturing processes of composites and their mechanical properties: a bibliography (1985-2003)," *Computational Materials Science*, vol. 31, no. 3–4, pp. 187–219, 2004.

[43] P. Mcallen and P. Phelan, "A method for the prediction of ductile fracture by central bursts in axisymmetric extrusion," *Proceedings of the Institution of Mechanical Engineers - Part C:*

Journal of Mechanical Engineering Science, vol. 219, no. 3, pp. 237–250, 2005.

[44] X. Xiao, "On the measurement of true fracture strain of thermoplastics materials," *Polymer Testing*, vol. 27, no. 2, pp. 284–295, 2008.

[45] M. Zhan, C. Gu, Z. Jiang, L. Hu, and H. Yang, "Application of ductile fracture criteria in spin-forming and tube-bending processes," *Computational Materials Science*, vol. 47, no. 2, pp. 353–365, 2009.

[46] D. T. Nguyen, J. G. Park, and Y. S. Kim, "Ductile fracture prediction in rotational incremental forming for magnesium alloy sheets using combined kinematic/isotropic hardening model," *Metallurgical and Materials Transactions A*, vol. 41, no. 8, pp. 1983–1994, 2010.

[47] X. Gao, T. Zhang, M. Hayden, and C. Roe, "Effects of the stress state on plasticity and ductile failure of an aluminum 5083 alloy," *International Journal of Plasticity*, vol. 25, no. 12, pp. 2366–2382, 2009.

[48] R. Ghajar, G. Mirone, and A. Keshavarz, "Ductile failure of X100 pipeline steel - experiments and fractography," *Materials & Design*, vol. 43, pp. 513–525, 2013.

[49] M. Wang, H. Yang, Z.-c. Sun, L.-g. Guo, and X.-z. Ou, "Dynamic explicit FE modeling of hot ring rolling process," *Transactions of Nonferrous Metals Society of China*, vol. 16, no. 6, pp. 1274–1280, 2006.

[50] M. R. Zhao, "Finite element simulation and optimization of ring rolling process," Master's thesis, Taiyuan University of Technology, Taiyuan, China, 2005.